Research Academy for Young Scientists

Kinematics and Fluid Mechanics Analyses of the Free Fall of Objects in Complex Fluids

Wilma Hall
hallwilma1908@gmail.com

under the direction of
Kasra Amini
KTH Royal Institute of Technology
Department of Engineering Mechanics
Linné Flow Centre (FLOW) and Fluid Physics Laboratory

July 12, 2023

*

Abstract

The forces acting on an object in free fall in a Newtonian fluid and the resulting flow fields are well understood subjects. Non-Newtonian fluids introduce more complexities and to study these effects both shadow-graphing and streak visualisation were performed on a variety of objects in four different non-Newtonian fluids and water as a reference. From the shadowgraph the velocity of a falling metal sphere was calculated and the terminal velocity used to gauge if the model of gravity, buoyancy and drag described the situation. A significant missing force against the direction of gravity was observed. This possibly due to elastic effects in the fluid. The flow field visualisations also presented interesting phenomenon such as negative wake and different formations of bubbles.

Acknowledgements

I would like to thank my mentor Kasra Amini for guiding me trough this project and I also want to thank Rays –for excellence and all of the people that have made this amazing program possible. I also want to give a big thank you to all of my fellow Rays students and xRays who have been helping me during the project. Further I want to thank the Åhlén-stiftelsen and Skolresurs who have been supporting Rays –for excellence.

Contents

1 Introduction

Gases and liquids are collectively referred to as fluids. They start to flow under shear stress, a force being applied tangential to the surface [1]. Fluids have a non rigid structures allowing them to to take the shape of their container and in the case of gases expand to fill the entire volume available. Liquids can for the purposes of this study bee considered incompressible so their density ρ is constant. The viscosity of the fluid η is its resistance to flow, in so called Newtonian fluids the viscosity is describes by the equation

$$\tau = \eta \frac{du}{dy} \,, \tag{1}$$

τ being the shear stress in Pa, the velocity of the upper layer of the surface being sheared $u(y)$, and η the viscosity. A fluid is considered Newtonian when the relationship between the shear stress and shear rate is linear which means that the viscosity is constant. [2].

When considering objects falling trough a fluid the fluid's density and viscosity affect the buoyancy force and drag force respectively. When an object falls through fluid it is pulled down by the gravitational force which is opposed by the drag and buoyancy forces.

1.1 Complex fluids

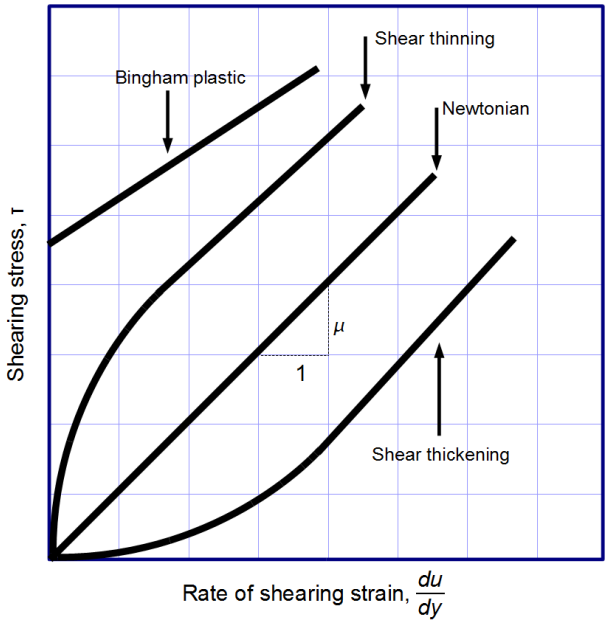

Figure 1: Graph of viscous regimes. [3]

Complex or non-Newtonian fluids have an non constant viscosity, which means that the magnitude of the shear stress and the deformation of the fluid have a non-linear relationship [1]. The viscosity depends on the cohesion of the fluid, how well molecular momentum is transferred in the different layers of the fluid [1]. Non-Newtonian fluids exhibit a wide range of viscous regimes, as shown in Figure 1. Some of the most common including shear thinning and shear thickening fluids. In shear thinning fluids the viscosity decreases as shear rate increases and inversely the viscosity increases with shear rate in shear thickening fluids [4]. Thixotropic fluids exhibit a kind of memory where their viscosity permanently diminishes with shear and rheopective fluids have the opposite effect where their viscosity permanently increases by shearing. Fluids that exhibit plasticity act like solids until a critical shear stress is reached under which they start to flow. In this study thixotropic and rheopectic fluids and effects are not considered.

1.1.1 Visco-elastic fluids

Elasticity is the ability of the material to return to its original form and resist forces deforming it. Many naturally occurring fluids like blood and mud also display this behavior [5]. Generally visco-elastic fluids are shear thinning [5] and their viscosity η as a function of shear rate $\dot{\gamma}$ can be described using the Carreau-Yasuda model (2)

$$\eta(\dot{\gamma}) = \eta_{\text{inf}} + (\eta_0 - \eta_{\text{inf}})[1 + (\lambda\dot{\gamma})^a]^{\frac{n-1}{a}}, \tag{2}$$

where η_{inf} is their viscosity at near infinite shear, η_0 is the viscosity at zero shear, λ is the relaxations time, n is the power law index and a is a dimensionless parameter [6].

1.1.2 Elasto-visco-plastic fluids

The characteristic property of elasto-visco-plastic fluids is that they have a yield stress τ_0 below which the fluid does not flow. Below it's yield stress the elasto-visco-plastic material acts more like a solid and it can deform elastically. These types of materials usually consist of long chain molecules which are cross-linked. Elasto-visco-plastic fluids can be both shear thickening and shear thinning. The Herschel-Bulkley model describes

the relationship between shear stress, yield stress, viscosity and shear rate,

$$\tau = \tau_0 + \kappa \cdot \dot{\gamma}^n \qquad \text{when } |\tau| \geq \tau_0 \tag{3}$$

$$\dot{\gamma} = 0 \qquad \text{when } \tau \leq \tau_0 \tag{4}$$

where τ is the shear stress, κ is the consistency index and n is the flow behavior index. The flow behavior index is $n > 1$ for shear-thickening fluids and $n < 1$ for shear thinning fluids [5].

1.2 Non dimensional numbers

Non dimensional numbers give important insight into the relation of different aspects of systems without the limitation of absolute values and units of measurements.

$$Re = \frac{\rho u h}{\eta_{rheo}} \tag{5}$$

is used to calculate the Reynolds number Re where ρ is the density of the fluid, u is the velocity, h is the characteristic length and η_{rheo} is the viscosity obtained by rheometry. The Reynolds number is a dimensionless number that describes the relationship of the viscous and inertial forces acting on the flow.

$$Wi = \frac{\lambda u}{h} \tag{6}$$

The Weissenberg Wi number describes the elasticity of the fluid. Where λ is elastic relaxation time u is the velocity and h the size of the object.

$$El = \frac{Wi}{Re} = \frac{\lambda \eta}{\rho h^2} \tag{7}$$

The elasticity number El describes the elasticity of the fluid independent from the inertia.

$$Bi = \frac{\tau_0 u}{\eta_{rheo} h} \tag{8}$$

The Birmingham number Bi describes the plasticity, the capacity of the material to permanently deform under stress which depends on the yield stress τ_0, the velocity, the characteristic lenght and the reference viscosity η_{rheo} measured based on the other variables.

1.3 Governing forces of an object in free fall

The main forces acting on an object in free fall are gravity F_G, buoyancy F_B and drag F_D, as visualised in Figure 2. The gravity is described by the equation

$$F_G = m \cdot g \tag{9}$$

m being the mass of the object and g the constant for the gravitational acceleration on earth $9.81\,\frac{\mathrm{m}}{\mathrm{s}^2}$. The buoyancy results from the energy needed to displace the objects volumes V worth of fluid against the gravitational force. It depends on the density of the fluid ρ, the volume of the object V and the constant g in accordance to the following equation

$$F_B = \rho V g. \tag{10}$$

The drag force of a sphere at a low Reynolds number $Re \lesssim 2000$ is described by the Stokes' law

$$F_D = 6\pi\eta r v \tag{11}$$

where η is the viscosity, r the radius of the sphere and v the velocity of the object [7]. At higher Reynolds numbers the drag increases with the square of the velocity and not linearly like in this case. In non-Newtonian fluids the drag is a function of both velocity and viscosity. In visco-elastic and elasto-visco-plastic fluids the elasticity and plastic effects can be expected to affect the how the object falls. These effects might bee seen as a modified drag or their own forces.

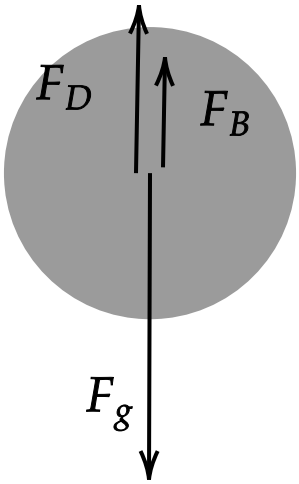

Figure 2: The forces acting on an object in free fall.

1.4 Aim of Study

The aim of the study is to observe the fluid flow around an falling object in visco-elastic- and elasto-visco-plastic fluid and to compare how well gravity, buoyancy and drag can describe the objects acceleration and terminal velocity, or if other non-modelled effects have an significant impact on fluid behaviour.

2 Method

For the purposes of observing the effects of visco-elasticity and elasto-visco-plasticity on an falling object in a complex fluids experiments with five fluids specified in Table 1 was prepared. Water was chosen as a reference point since its flow mechanics are well known due to it being an Newtonian fluid. Two different concentrations of a polyacrylamide solution (PAA) were chosen as the visco-elastic fluid and two concentrations of a carpobol solution for the elasto-visco plastic fluid. These fluids were chosen in part because of they are clear and see trough making optical observations easy.

2.1 Material preparations

The polyacrylamide solution was made using the anionic polymer FLoPAM AN 934 SH made by SNF, which has a very high molecular weight. The powder was mixed with water

Table 1: The fluids used for the experiment

Name	Fluid	Concentration
Control	Water	
VEF I	PAA	5000 ppm
VEF II	PAA	10 000 ppm
EVP I	Carpobol	0.1 %
EVP II	Carpobol	0.2 %

in an 25 L container. The solution was mixed with a modified handheld cement mixer for approximately 12–16 h until no polymer clumps were visible and the solution was assumed uniform. Two concentrations of the solution were prepared 5000 ppm and 10 000 ppm for the experiment.

For the carpobol solution the carbomer powder Carpobol NF 980 by Lubrizol Corporation was mixed with water. The mixing was done in 25 l batches with a modified handheld cement mixer. The solution was mixed for about 30 minutes and then allowed to rest for about the same time so that bubbles could escape. After mixing the polyacrylic acid with water, 2.3 times the weight of the polymer powder of sodium hydroxide (NaOH) was added to the mix to neutralise it while gently mixing, increasing its capacity to absorb water in order to form a yield stress fluid.

2.2 Rheology

The rheometry was performed on an Anton Paar Modular-Compact-Rheometer (MCR) 702e Space. For the PAA a polished plate and an 1° cone with a 93 µm truncation was used. The pieces are positioned so that if the cone had it's tip it would touch the plate and the torque on the cone is measured when the plate is rotated to get the shear stress and viscosity. With the CP a sand blasted plate with the roughness of 7 µm was used in combination with a cone with a 101 µm truncation was used. The rough plate was used for the carpobole since it is known to have significant wall slip [8]. The measurements were done with shear rates ranging from 10^{-3} to 10^{3} with 6 points per decade. The data was recorded after the values reached a steady reading at the given shear rate. [6]

The rheometry results for the two PAA solutions match the Carreau-Yasuda model

equation: 2 well. The measurements with the 0.1% carpobole however doesn't follow the Hershel-Bulkley model that well Figure: (3) and most importantly doesn't seem to have the characteristic plateau and the lower end of the shear rate. This could just mean that concentration of the polymer doesn't reach the necessary limit for the fluid to truly act in accordance with the model or that the plateau exists at lower shear than measured.

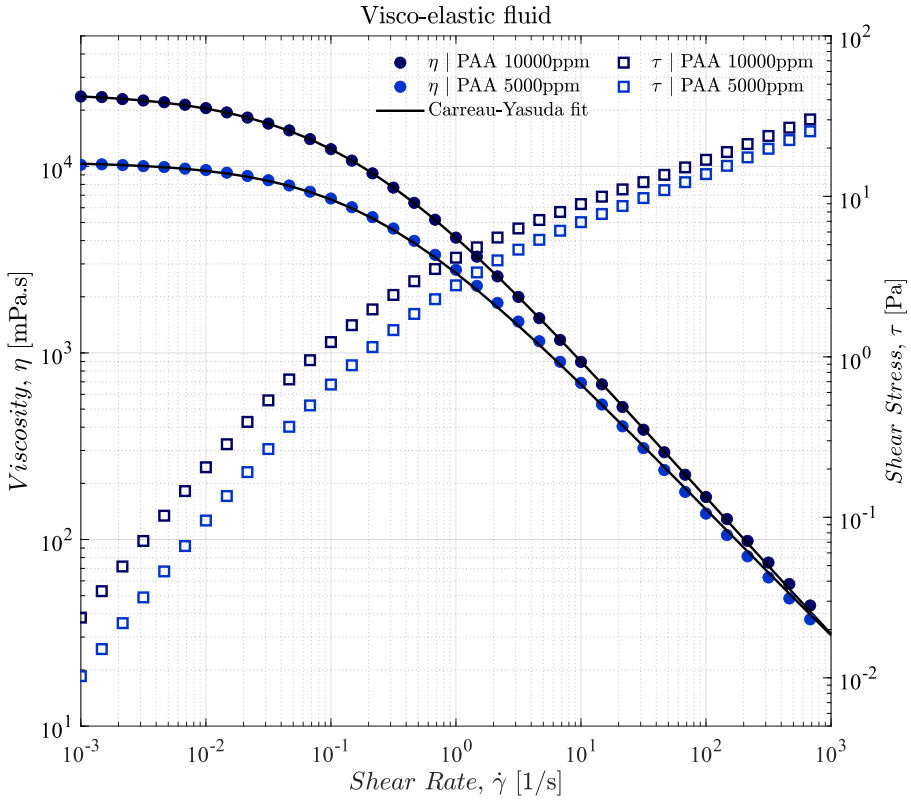

(a) The viscosity and shear stress of polyacrylamide

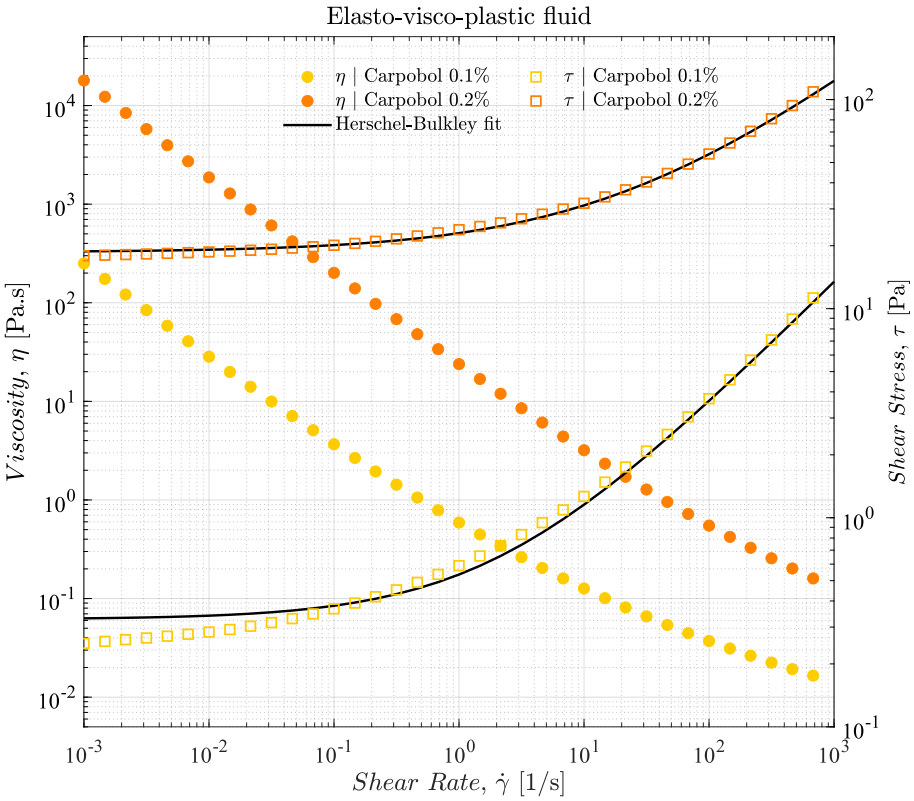

(b) The viscosity and shear stress of carpobole

Figure 3: The rheometry curves for Carpobole and PAA

2.3 Experimental setup

The primary object used for the experiments is a metal sphere with the radius of 10 mm and a mass of 32.2 g. Three different cylinders were also used to explore the effect of different geometries on the flow field. The cylinders also provided an approximation of a 2D model for the streak visualisation. The small cylinder has a radius of 12 mm, height 24 mm and mass of 84.0 g, the medium cylinder a radius of 12 mm, height of 36 mm and mass 126.3 g and the large cylinder a radius of 3.5 mm, height of 70 mm and a mass of 81.0 g. A standard golf ball was also used with the radius 21 mm and weight 45.7 g.

Figure 4: Objects used for the experiment

2.3.1 Shadowgraph

Shadowgraphing was used to follow the movement of the falling object trough the liquid Figure 5 and determine its velocity. The experiment was performed in a dark room so that the bright light behind the container would show the shadow of the falling object. Frame rates ranging from 100 fps to 500 fps were used in filming the shadowgraph and the location of the object was determined either by millimeter paper at the back of the container or a stripe of it on the front edge fort the fluids that were not transparent enough.

2.3.2 Streak visualisation

To visualize the flow field around the falling object particles with the diameter (50 µm) were mixed into the fluid and a laser sheet perpendicular to the camera line was used to illuminate the particles. Longer exposure times on the camera were used so that streaks

Figure 5: The shadow graph setup

showing the movement of the particles were created. To accommodate for the different velocities and experiment with optimal exposure for different properties of the flow frame rates from 100 fps to 5 000 fps were used.

2.4 Correction of measurement errors

Since the measurements for the position of the object were made based on video from a camera that was stationary and close to the fluid container the further they are from the horizontal camera line from the camera the more skewed they are. The camera was positioned so that the direct line of sight was in the middle of the container. The light refraction when passing from air to the liquid is also considered, table: 5.

The angle between the horizontal camera line and the beam direction is the same as the angel of incidence so both are denoted i and the angel of refraction r. The distance from the camera to the front of the setup is denoted d, the half-height of the visible area of liquid in the container H, the width of the container l and the distance from the

horizontal camera line to the point where the light enters the fluid is B. The correction

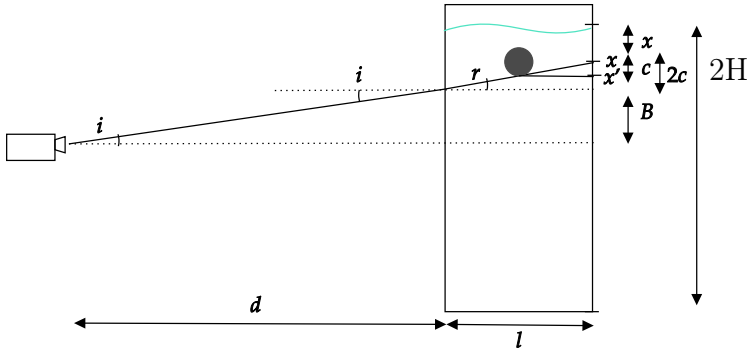

Figure 6: Visualisation of the measurement correction process.

c is added or subtracted from the original x position of the object to obtain the new corrected position x'. The action to obtain x' depends on whether the scale on the back or the front of the container was used and whether the measurement was made above or below the horizontal camera line.

$$c = \frac{l}{2} \tan\left(\arcsin\left(\frac{n_w}{n_a} \sin\left(\arctan\left(\frac{H - 2c - x_0}{d}\right)\right)\right)\right) \tag{12}$$

$$c \approx \frac{l}{2} \tan\left(\arcsin\left(\frac{n_w}{n_a} \sin\left(\arctan\left(\frac{H - x_0}{d}\right)\right)\right)\right) \tag{13}$$

The equation 12 that describes the needed corrections from the known variables was simplified to equation 13 since in comparison to H, d and x_0 the $2c$ is way smaller and can be considered insignificant.

3 Results and Discussion

3.1 Kinematics

As the velocity of the metal sphere falling trough VEF1 stabilizes at the end it can be assumed that it has reached its terminal velocity. As the sphere was placed at the fluid surface and then let go it can be assumed that its initial velocity was zero. The average of the later data points is used to get rid of the noise in the data and in the cases where the velocity does not appear to change much anymore it is assumed to be the terminal velocity. The terminal velocity is used to calculate the sum of the forces assumed to be

Force	(N)
Gravity	0.316
Buoyancy	-0.041
Drag	-0.028

Table 2: The magnitude of the forces calculated using the average velocity at the end.

present, gravity, buoyancy and drag. A table with more details on the calculations and parameters can be found in appendix A.

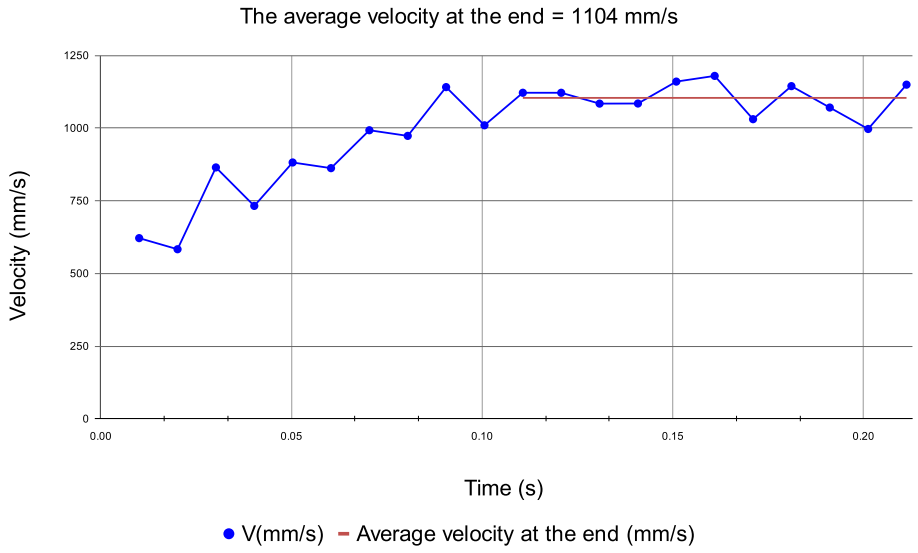

Figure 7: The measured velocity and the average of the terminal velocity of the metal sphere in VEF1.

$$\Sigma F = F_G + F_B + F_D$$

$$\Sigma F = mg - \rho V g - 6\pi\eta r v$$

$$\Sigma F = mg - \rho V g - 6\pi(\eta_{\text{inf}} + (\eta_0 - \eta_{\text{inf}})[1 + (\lambda\dot{\gamma})^a]^{\frac{n-1}{a}})rv$$

$$\Sigma F = 0.2470N$$

The sum of the forces 0.2470 N, which is significant for the forces present and suggest that the object would continue to accelerate and that it has not reached its terminal velocity. However the terminal velocity was observed and as such there must be an force that was not accounted for resulting from elasticity of the fluid.

3.2 Flow fields

Water has been used as a Newtonian reference case. As the case in water has a relatively higher Reynolds number in the order of 10^4 the wake shows some instabilities figure: 8. The low viscosity also means that the majority of the field is not effected and the wake is narrow.

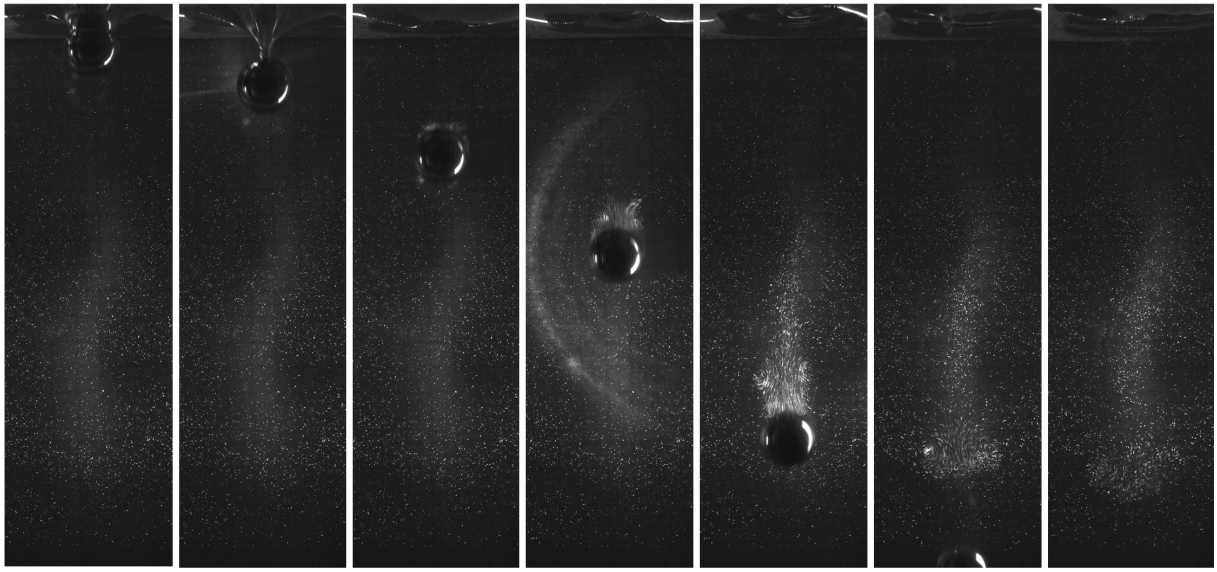

Figure 8: The reference case of a flow field around a sphere in water

In the Figure 9 it can be observed that the wake is considerable wider than in water as the higher viscosity leads to the movement spreading the wake is also more symmetrical than in water as the viscosity dampens the inertia in the liquid.

A sphere causes a different flow field than a cylinder since in a sense the cylinder when falling perpendicular to the ground is an approximation for a 2D model with a circle. In the Figure 10 it can be seen how the particles visualising the flow field moving out of the plane as they flow past the sphere.

In the EVPs the yield stress and flow lead to a low pressure point on the backside of a cylinder where bubbles tend to form after the breaking of the surface as shown in Figures 11 and 12. The plasticity and elasticity also mean that the surface stretches far before breaking as seen in Figure 12.

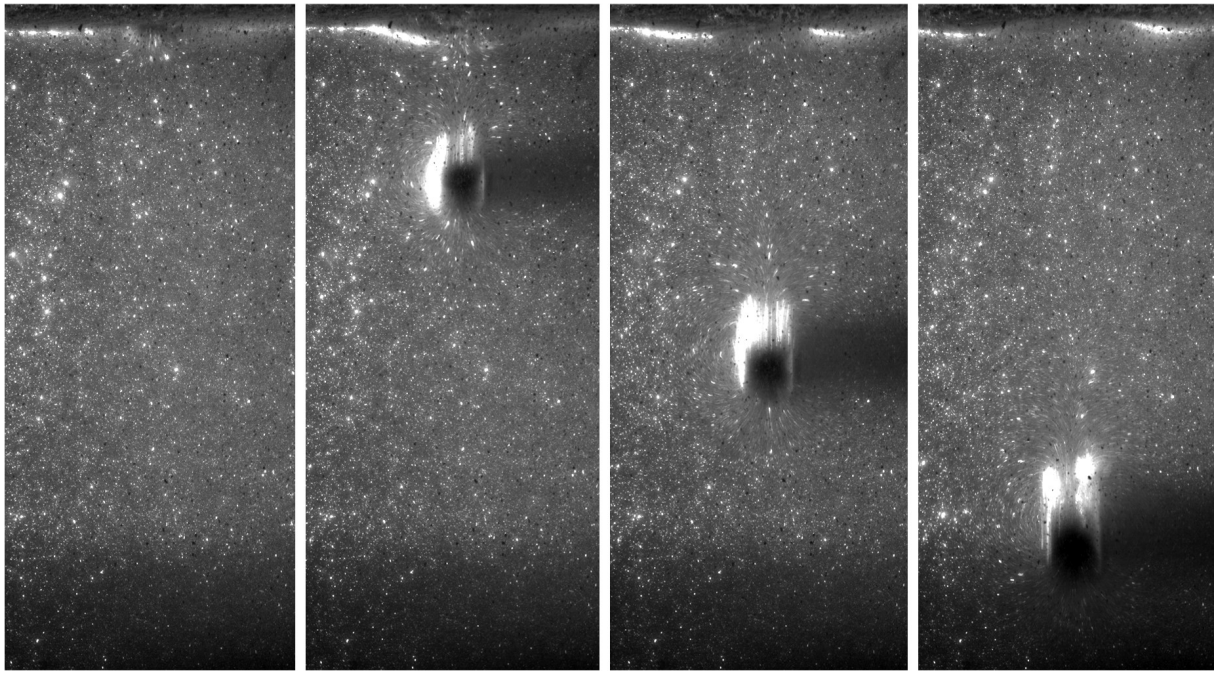

Figure 9: The flow field around a cylinder in EVP2

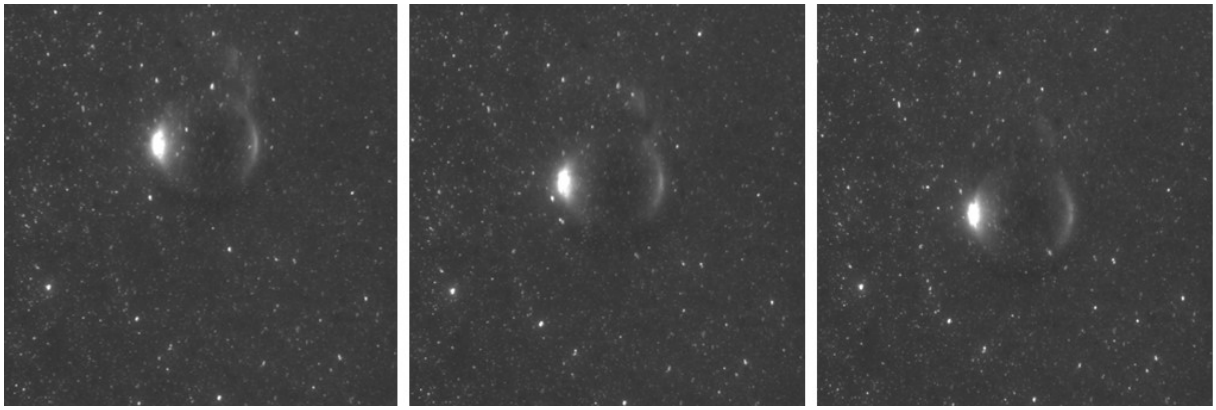

Figure 10: The 3D aspect of a flow field around a sphere

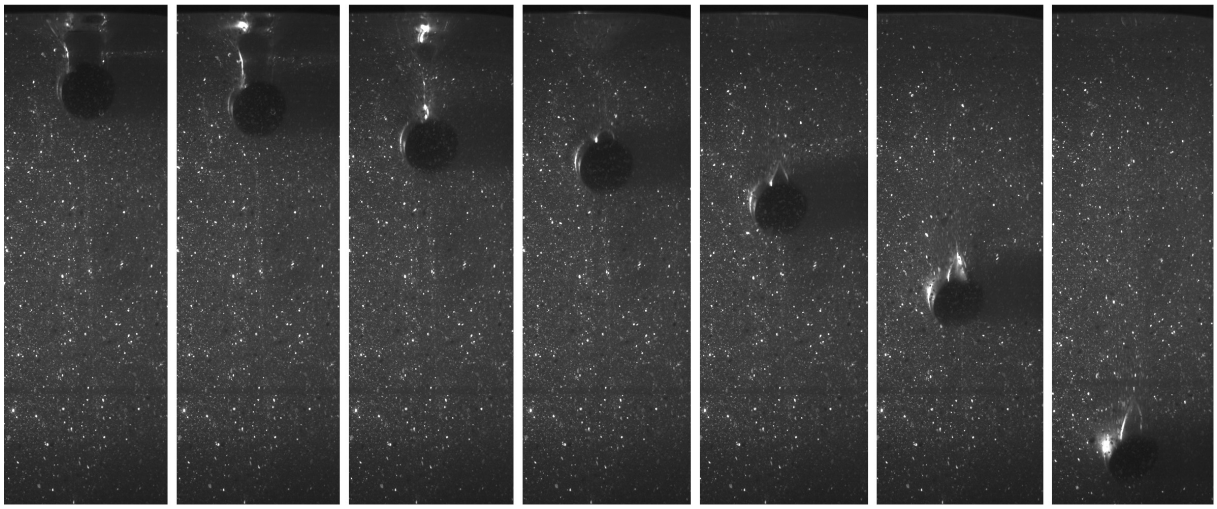

Figure 12: Breaking of the surface and formation of bubbles in EVP1.

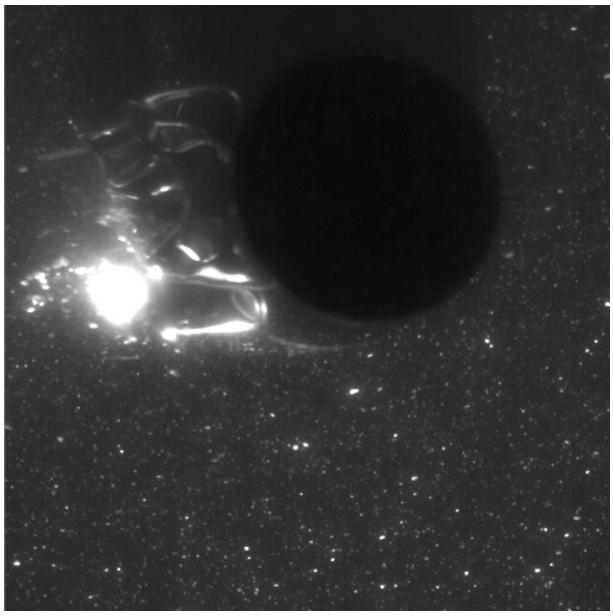

Figure 11: Formation of bubbles around a cylinder in an elasto-visco-plastic fluid

In EVP1 shown in Figure 15 which is less viscous than EVP2 a complex and asymmetrical wake forms where the vortexes spread unevenly as the yield stress threshold ads a dampening effect in certain areas. The wake spreads quite far from the path of the object in contrast to Figure 17 of VEF.

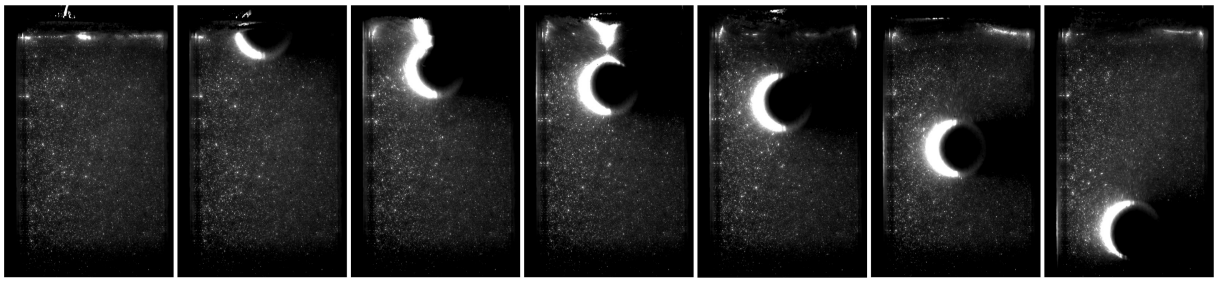

Figure 13: F

Figure 14: Symmetry of the wake around a golf ball in EVP1.

The Figure 14 shows a symmetrical creeping flow around the falling golf ball as it has a lower density the inertial forces involved are smaller so that the Reynolds number is lowing and a Stokes flow takes place around the ball.

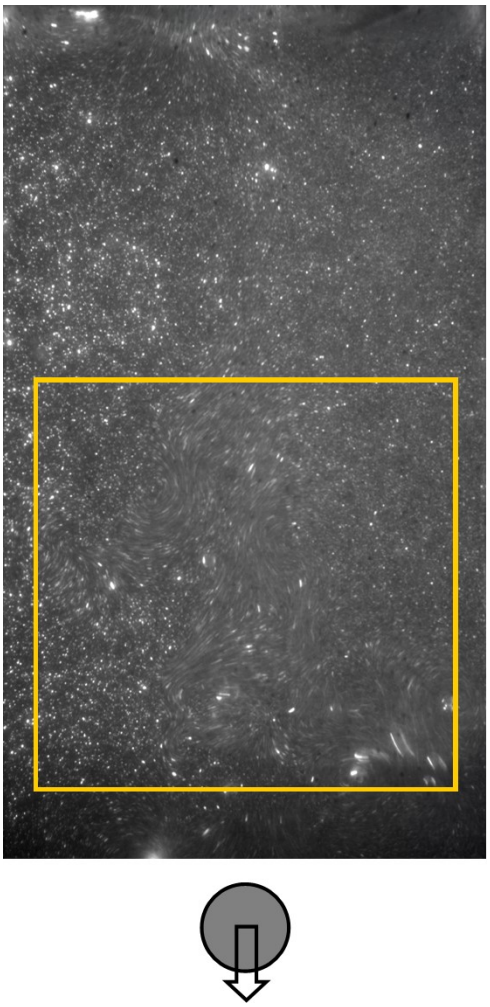

Figure 15: The complex wake of an EVP

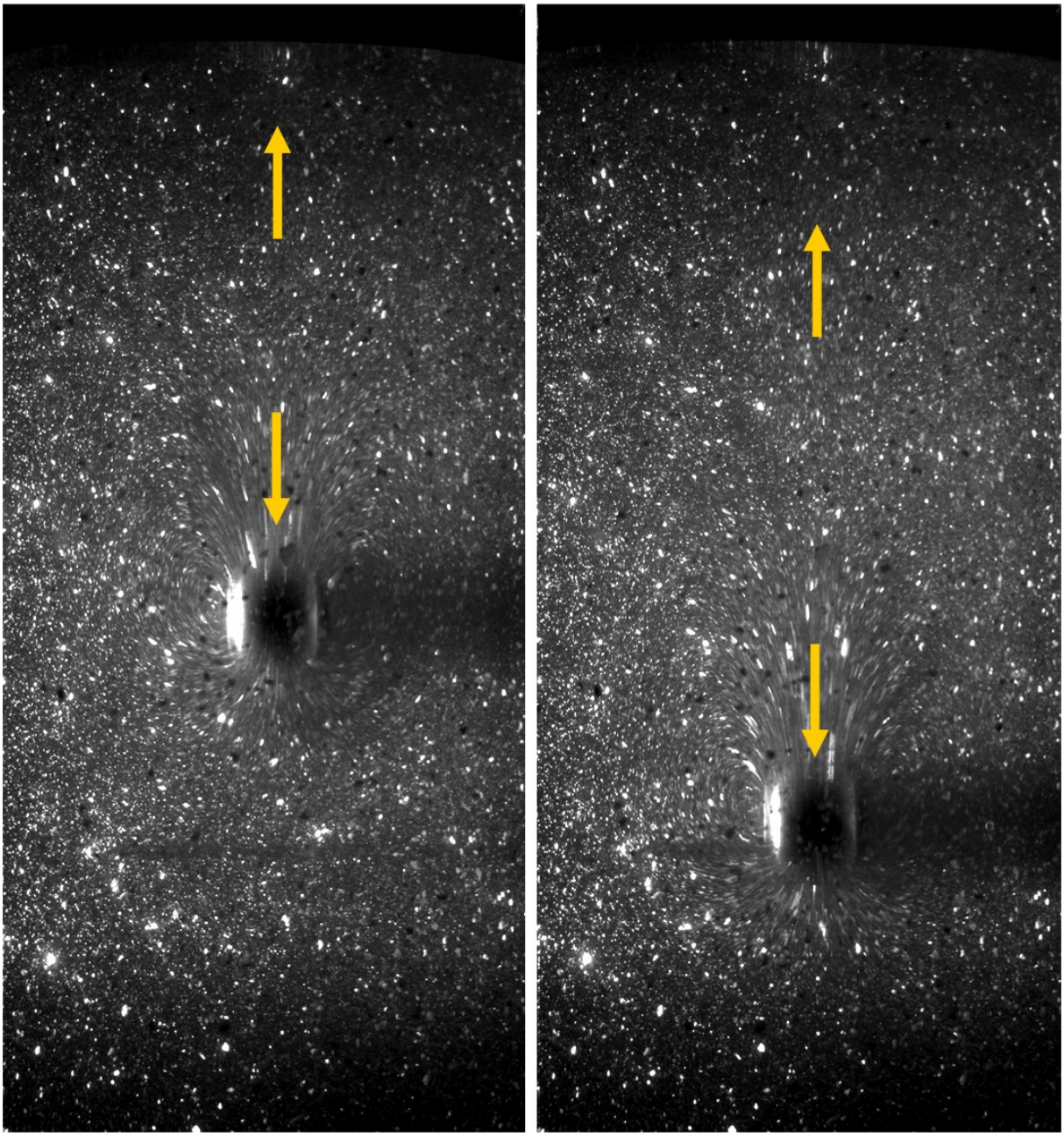

Figure 16: The negative wake in EVP2.

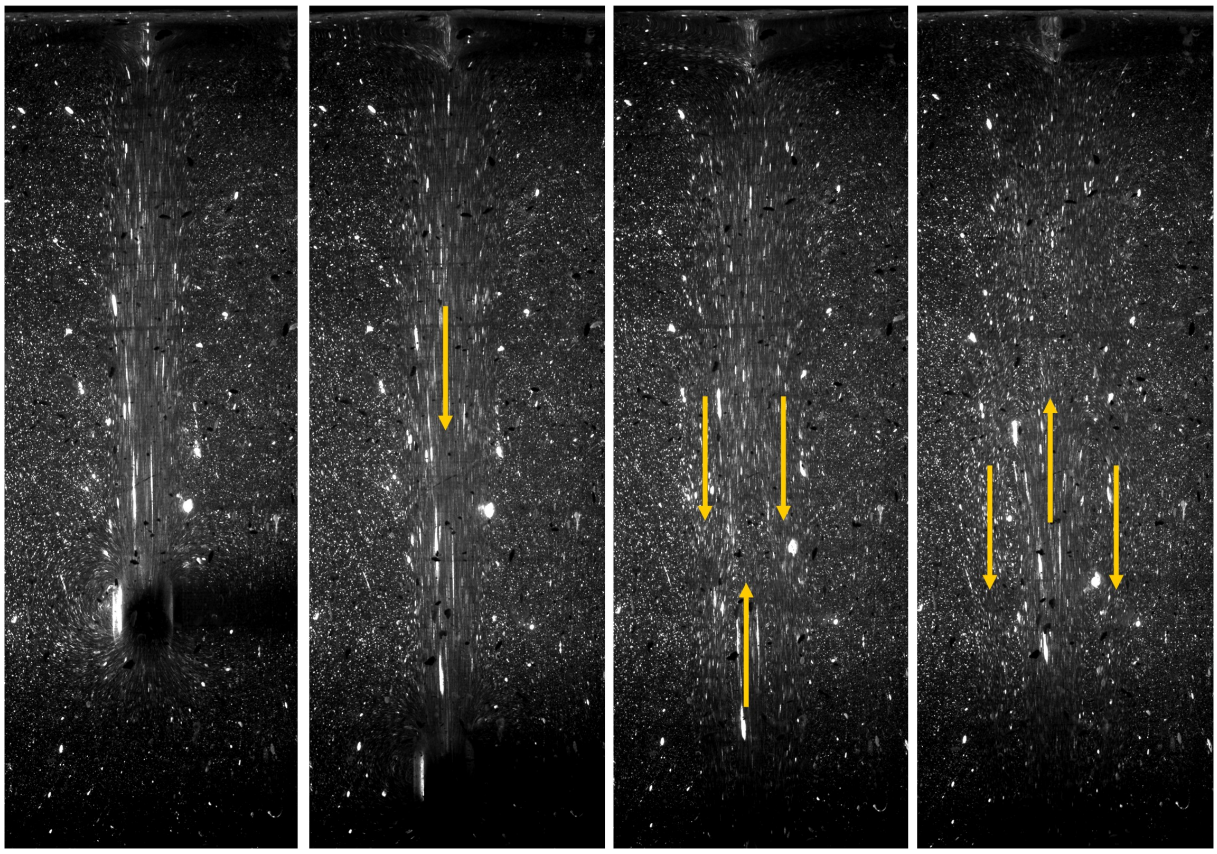

Figure 18: Reverse wake in a VEF.

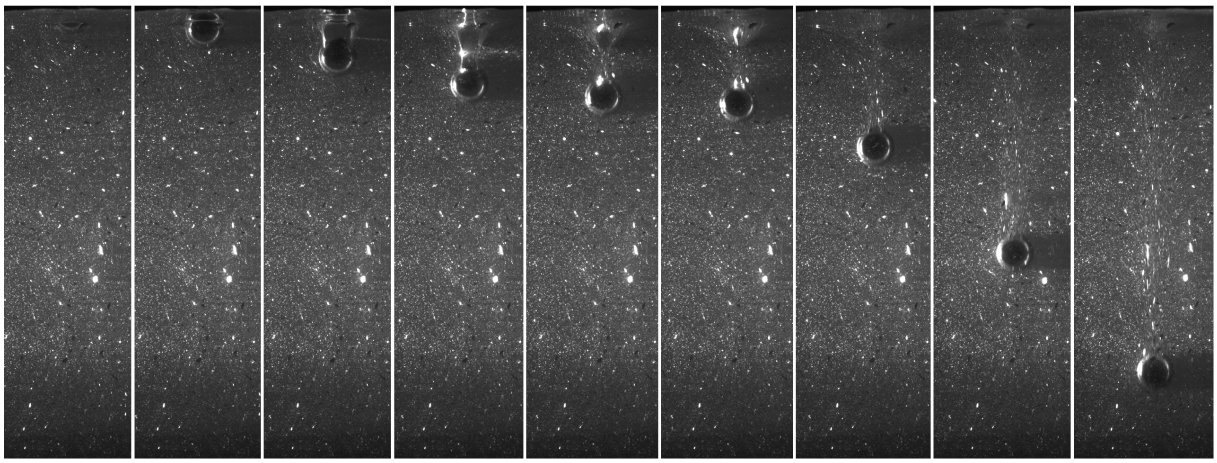

Figure 17: Long elastic chain wake in VEF1.

The Figures 16 and 18 show a negative wake, the fluid moves in the opposite direction of the falling object. In Figure 18 the start of the negative wake can bee seen. The wake is also long as the interconnected polymers elastically pull on the fluid.

In elastic fluids the elastic effects in certain situations outweigh other forces such as the surface tension resulting in a moving bubble having a sharp tail like in Figure 19.

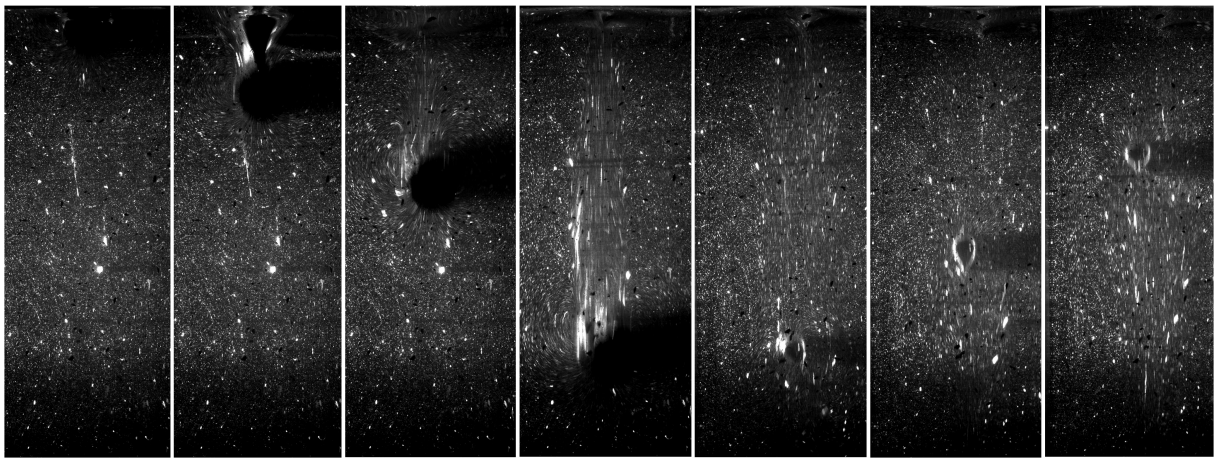

Figure 19: A bubble with a sharp tail.

4 Conclusion

The kinematics and calculations of forces on the falling sphere it can be said that the elasticity of the fluid exerts a significant force on a falling object greatly reducing its terminal velocity. For further studies into how this force can be determined and how to describe its effects for applications such as mixing in production of different products could be considered. Ribeiro et al [9] have already studied the effects of elasticity in flow past a cylinder in a duct the visco-elastic properties have also been studied with higher impact speeds by Goede et al [10]. In the experiments further kinematic data on different fluids and geometries of objects were made and on the basis of them it would be possible to calculate better predictions for a wider range of behaviours. These have already been studied by Shiau [11] and those findings could be useful.

Different flow phenomena like reverse wake and bubble formation behind a cylinder where observed in the streak visualisation. These could be further studied by examining the flow field visualisations closer and modeling it. The flow fields could also be better interpreted to vector fields using the length of streaks and exposure time to get more precise information on the fluids movements.

References

[1] V. L. Streeter, *Fluid Mechanics by Streeter*, vol. 3. McGraw Hill Book Company, international student ed., 1958.

[2] F. White, *Fluid Mechanics 8th edition direct textbook*. McGraw Hill Education, 8 ed., 2016.

[3] Dhollm, "Viscous regimes chart," 2010.

[4] S. L. H. P. A. Putaiao, "Non-newtonian fluids," 2010.

[5] S. Zade, *Experimental studies of large particles in Newtonian and non-Newtonian fluids*. PhD thesis, KTH Roayl Institute of Technology, 2019.

[6] K. Amini, V. K. Gowda, S. Saoncella, L. Brandt, S. Bagheri, O. Tammisola, and F. Lundell, "Experimental study of the effects of viscoelasticity and surface structures on the near-wall velocity profiles using doppler optical coherence tomography (d-oct)[paper in preparation]," 2023.

[7] Wikipedia contributors, "Drag (physics) — Wikipedia, the free encyclopedia," 2023. [Online; accessed 12-July-2023].

[8] J. Piau, "Carbopol gels: Elastoviscoplastic and slippery glasses made of individual swollen sponges: Meso- and macroscopic properties, constitutive equations and scaling laws," *Journal of Non-Newtonian Fluid Mechanics*, vol. 144, no. 1, pp. 1–29, 2007.

[9] V. Ribeiro, P. Coelho, F. Pinho, and M. Alves, "Viscoelastic fluid flow past a confined cylinder: Three-dimensional effects and stability," *Chemical Engineering Science*, vol. 111, pp. 364–380, 2014.

[10] G. T.C., B. K.G., and B. D, "High-velocity impact of solid objects on non-newtonian fluids," *Scientific reports*, 2019.

[11] T. Shiau, *Drag on a Cylinder in a Viscoelastic Stokes Flow*. PhD thesis, University of Toronto, 2014.

A Case specifications

Specifications for the calculations on dimensionless numbers and viscosities. `https://docs.google.com/spreadsheets/d/1WvThjh3h6ATjzSvrprjVAgvwVdejItWlBbRfCH6gygo/edit?usp=sharing`

Table 3: Case specifications: shadowgraph

Fluid	Frame rate ($\frac{1}{s}$)	Object Shape	Object dimensions	Case number
Water	100	Sphere	$r = 10mm$	Case 11
VEF1	400	Sphere	$r = 10mm$	Case 21
VEF1	400	Cylinder	$r = 7mm$, $h = 70mm$	Case 22
VEF2	400	Sphere	$r = 10mm$	Case 26
VEF2	400	Cylinder	$r = 7mm$, $h = 70mm$	Case 28
EVP1	500	Sphere	$r = 10mm$	Case 35
EVP1	500	Cylinder	$r = 7mm$, $h = 70mm$	Case 37
EVP1	500	Golf ball	$r = 21mm$	Case 39
EVP2	500	Sphere	$r = 10mm$	Case 45

Table 4: Case specifications: Streak visualisation

Fluid	Frame rate ($\frac{1}{s}$)	Object Shape	Object dimensions	Case number
Water	100	Sphere	$r = 10mm$	Case 1
Water	500	Sphere	$r = 10mm$	Case 5
Water	750	Sphere	$r = 10mm$	Case 7
VEF1	500	Sphere	$r = 10mm$	Case 14
VEF1	100	Sphere	$r = 10mm$	Case 15
VEF1	100	Cylinder	$r = 12mm$, $h = 24mm$	Case 16
VEF1	100	Cylinder	$r = 7mm$, $h = 70mm$	Case 17
VEF1	100	Golf ball	$r = 21mm$	Case 18
VEF1	3000	Sphere	$r = 10mm$	Case 19
VEF2	100	Sphere	$r = 10mm$	Case 23
VEF2	100	Cylinder	$r = 12mm$, $h = 24mm$	Case 24
VEF2	100	Cylinder	$r = 7mm$, $h = 70mm$	Case 25
EVP1	100	Sphere	$r = 10mm$	Case 29
EVP1	500	Sphere	$r = 10mm$	Case 30
EVP1	3000	Sphere	$r = 10mm$	Case 31
EVP1	3000	Cylinder	$r = 12mm$, $h = 36mm$	Case 32
EVP1	100	Cylinder	$r = 12mm$, $h = 36mm$	Case 33
EVP1	100	Golf ball	$r = 21mm$	Case 34
EVP2	100	Sphere	$r = 10mm$	Case 40
EVP2	100	Cylinder	$r = 12mm$, $h = 36mm$	Case 42
EVP2	5500	Sphere	$r = 10mm$	Case 43
EVP2	3000	Cylinder	$r = 12mm$, $h = 24mm$	Case 44

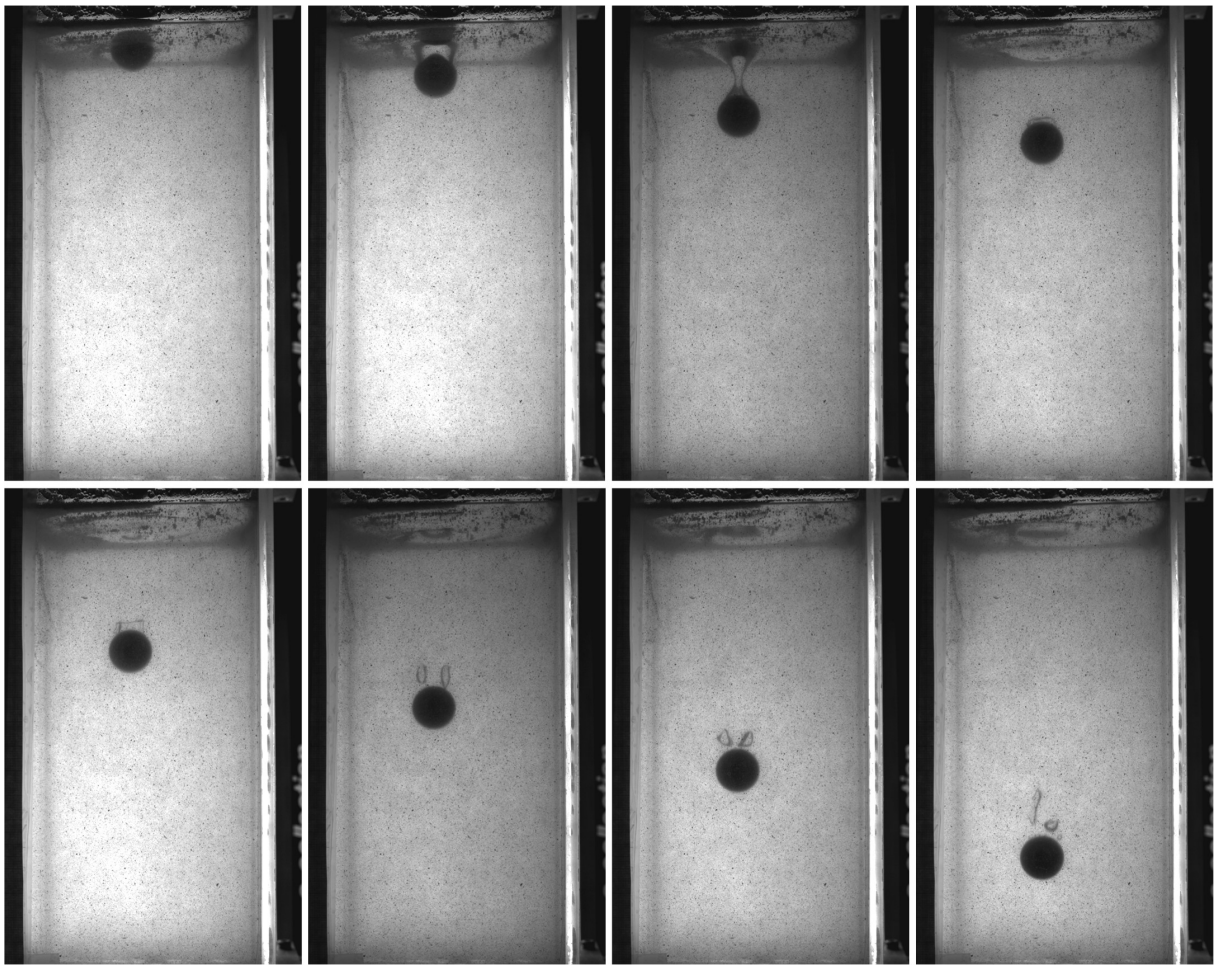

Figure 20

B Further video and image results

Case 18, Video of golfball that stops and then continues to fall. `https://drive.google.com/file/d/1qOYHqMBznCtCrHCO3w076es25EX9eTHF/view?usp=sharing`

C Calculation of measurement error.

The refractive indexes used in the calculation are specified in the following table.

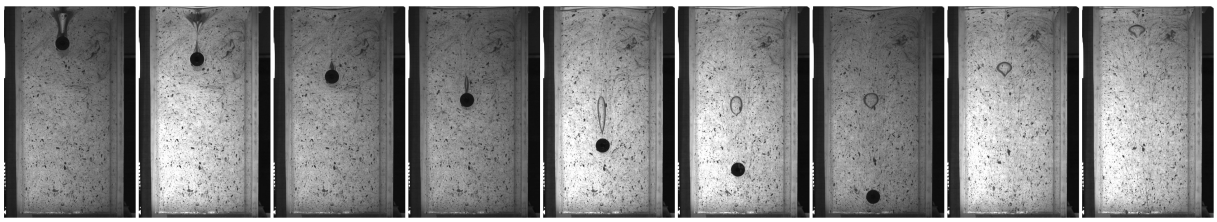

Figure 21

Table 5: Refractive indexes

Fluid	Refractive index n
Water	$1,33$
PAA	$1,33$
CP	$1,44$

The equation to calculate the measurement error were derived as follows.

$$B = H - x_0 - 2c$$

$$\tan(i) = \frac{B}{d} \longrightarrow i = \arctan\left(\frac{B}{d}\right)$$

$$\tan(r) = \frac{2c}{l} \longrightarrow c = \frac{l}{2} \cdot \tan(r)$$

$$\sin(r) = \frac{n_{fluid}}{n_{air}} \cdot \sin(i) \longrightarrow r = \arcsin\left(\frac{n_{fluid}}{n_{air}} \cdot \sin(i)\right)$$

$$c = \frac{l}{2} \tan\left(\arcsin\left(\frac{n_w}{n_a} \sin\left(i\right)\right)\right)$$

$$c = \frac{l}{2} \tan\left(\arcsin\left(\frac{n_w}{n_a} \sin\left(\arctan\left(\frac{H - 2c - x_0}{d}\right)\right)\right)\right)$$

$$c \approx \frac{l}{2} \tan\left(\arcsin\left(\frac{n_w}{n_a} \sin\left(\arctan\left(\frac{H - x_0}{d}\right)\right)\right)\right)$$